The Effect of Relativistic Kinematics on the Pion-Dressed Deuteron

Mikkel Moth Billing

Bachelor's Project

Department of Physics and Astronomy

Aarhus University

Supervisor: Dmitri Fedorov

June 2026

Abstract

This report investigates the deuteron using a nuclear model with explicit mesons, describing the system as a superposition of a bare neutron-proton state and a dressed nucleon-nucleon-pion state. Transitions between these states generate the effective nuclear attraction. The spatial wavefunctions are evaluated using the Stochastic Variational Method and a basis of correlated shifted Gaussians. The model is calibrated by tuning a nucleon interaction range and a pion-nucleon coupling strength to reproduce the experimental deuteron binding energy and charge radius.

After establishing the classical baseline, the effect of relativistic kinematics is evaluated. Because the explicitly modeled pion is lighter than the nucleons, it reaches relativistic velocities inside the nucleus. Replacing the classical kinetic energy operators with exact relativistic counterparts reveals a binding energy shift of approximately 4.5 MeV for the pion, compared to a 0.4 MeV shift for the heavier nucleons. Ultimately, a mixed kinematic model, applying classical operators to the nucleons and a relativistic operator to the pion, captures the majority of the physical correction while minimizing computational cost, providing an efficient framework for future multi-meson research.

Resumé

Dette projekt undersøger deuteronen ved hjælp af en kernemodel med eksplicitte mesoner, hvor systemet beskrives som en superposition af en bar neutron-proton-tilstand og en klædt nukleon-nukleon-pion-tilstand. Overgange mellem disse tilstande skaber den effektive kernekraft. De rumlige bølgefunktioner evalueres med den stokastiske variationsmetode (SVM) ved brug af en basis af korrelerede forskudte Gauss-funktioner. Modellen kalibreres ved at justere rækkevidden for nukleonvekselvirkningen og koblingsstyrken mellem pion og nukleon for at reproducere deuteronens eksperimentelle bindingsenergi og ladningsradius.

Efter at have etableret den klassiske basislinje evalueres effekten af relativistisk kinematik. Da den eksplicit modellerede pion er lettere end nukleonerne, opnår den relativistiske hastigheder inde i kernen. Udskiftning af de klassiske operatorer for kinetisk energi med eksakte relativistiske ækvivalenter afslører et energiskift på cirka 4.5 MeV for pionen, sammenlignet med et skift på 0.4 MeV for de tungere nukleoner. Samlet set fanger en blandet kinematisk model, med klassiske operatorer for nukleonerne og en relativistisk operator for pionen, størstedelen af den fysiske korrektion, samtidig med at beregningstiden minimeres. Dette udgør en effektiv ramme for fremtidig forskning i multimeson-systemer.

Contents

1 | Introduction

The deuteron is the simplest bound nucleus, consisting of just one proton and one neutron. Due to its simplicity, it serves as the natural starting point for investigating the strong nuclear force. While standard nuclear models describe this force using effective potentials fitted to experimental data, this project utilizes the nuclear model with explicit mesons (MEM). Working within the one-pion approximation, the physical deuteron is modeled as a quantum superposition of a bare neutron-proton state and a dressed nucleon-nucleon-pion state. Transitions between these states generate the effective attraction that binds the nucleus.

Solving the Schrödinger equation for this multi-channel system requires efficient computational techniques. This is achieved by employing the Stochastic Variational Method (SVM) utilizing a basis of correlated shifted Gaussians. This choice of basis is advantageous because it provides analytical matrix elements for the overlaps and spatial interactions, reducing computation time. By optimizing the widths and spatial shifts of these Gaussians, the basis can dynamically capture the exact spatial structure of the loosely bound deuteron.

The pions have a mass of approximately 140 MeV, which is significantly lighter than the 940 MeV nucleons. Consequently, the pion reaches relativistic speeds within the nucleus, meaning the classical kinetic energy operator $p^2/2m$ may lack sufficient accuracy. The primary objective of this project is to quantify this relativistic correction. By evaluating the Hamiltonian using both the classical operator and the exact relativistic operator, $\sqrt{p^2 + m^2} - m$, the resulting energy shift is isolated. This comparison is performed independently for the heavy nucleons and the light pion to determine where relativistic kinematics are necessary.

2 | Deuteron System

In this project, the deuteron is modeled as bound by a single pion by expressing it as two subsystems: one with the bare deuteron core consisting of a proton and a neutron, and a second system that also contains a pion. This two-channel approach allows for the calculation of, how the pion mediates the attraction between nucleons, effectively providing a pion-exchange model without directly solving the full three-body problem.

The spatial wavefunction can be described as a vector of the two systems

$$\psi = \begin{pmatrix} \psi_{pn}(\boldsymbol{r}_p, \boldsymbol{r}_n) \\ \psi_{pn\pi}(\boldsymbol{r}_p, \boldsymbol{r}_n, \boldsymbol{r}_\pi) \end{pmatrix}, \tag{1}$$

where $\boldsymbol{r}_i$ is the coordinate vector of the i'th particle. This represents a two-particle and a three-particle system, which are subsequently reduced to $(N-1)$ systems using Jacobi center-of-mass coordinates in Chapter 3.

To couple the bare pn channel to the $pn\pi$ channel, the pion emission/absorption operator W is introduced. It acts between the two subspaces and decides both the allowed transitions and their amplitudes.

With this, a Hamiltonian describing the system can be constructed. The top-left K_{pn} is the kinetic energy of just the bare nucleon pair. The bottom-right $K_{pn\pi}+m_\pi$ is the kinetic energy plus rest mass of the three-body system with the pion. The off-diagonal W blocks allow the system to transition between these two states.

$$H = \begin{pmatrix} K_{pn} & W \\ W^\dagger & K_{pn\pi} + m_\pi \end{pmatrix}. \tag{2}$$

Only the kinetic energy is modeled explicitly, as the W operator accounts for the nucleon-nucleon potential. The Coulomb interaction between the particles is neglected in this model, since the effect of kinetic energy is the primary focus, and the Coulomb potential is assumed to have a minimal effect on the strongly bound core.

2.1 Variational principle

The binding energy is the energy gained when nucleons bind together. It equals the energy difference between a separated nucleon pair (zero reference) and the bound deuteron state. Since the chosen Hamiltonian has zero energy at infinite separation, the ground state energy E_0 is negative, and the binding energy is defined as $E_d = -E_0$.

To determine the binding energy of this system, the variational principle can be used to find an upper bound for the ground state energy. The variational principle states that for any spatial wavefunction Ψ, the expectation value of H satisfies

$$E = \frac{\langle \Psi | H | \Psi \rangle}{\langle \Psi \mid \Psi \rangle} \geq E_0, \tag{3}$$

where Ψ is an eigenstate of H with eigenvalue E_0 [1]. This implies that any trial wavefunction will give an energy that is higher than (or equal to) the true ground state energy. Therefore, by evaluating multiple wavefunctions and selecting the one with the lowest energy, the true ground state is gradually approached.

With this, a system of linear combinations of wavefunctions can be built and minimized to find an approximate ground state wavefunction:

$$\Psi = \sum_{i=0}^{n} c_i \psi_i(a_i), \tag{4}$$

where the parameters a_i tune each wavefunction to push the energy as low as possible. To find the coefficients c_i, the Hamiltonian matrix $\mathcal{H}$ and overlap matrix $\mathcal{N}$ are constructed from the basis functions, and the generalized eigenvalue problem is solved:

$$\mathcal{H}c = E\mathcal{N}c, \tag{5}$$

where

$$\mathcal{H}_{ij} = \langle \psi_i(a_i) | H | \psi_j(a_j) \rangle, \quad \mathcal{N}_{ij} = \langle \psi_i(a_i) \mid \psi_j(a_j) \rangle. \tag{6}$$

The lowest eigenvalue E of this generalized eigenvalue problem represents an upper bound on the ground state energy. The numerical solution method is discussed in detail in Chapter 6.4.

3 | Jacobi Transformation

To reduce the dimensionality of the required calculations, a center-of-mass Jacobi transformation is introduced. The Jacobi matrix is defined by

$$J = \begin{pmatrix} \frac{m_1}{M_1} & -1 & 0 & ... & 0 \\ \frac{m_1}{M_2} & \frac{m_2}{M_2} & -1 & ... & 0 \\ \vdots & \vdots & \vdots & \ddots & \vdots \\ \frac{m_1}{M_N} & \frac{m_2}{M_N} & ... & \frac{m_{N-1}}{M_N} & \frac{m_N}{M_N} \end{pmatrix} \tag{7}$$

where $M_n = \sum_{i=1}^{n} m_i$. The last row describes the center-of-mass coordinates. This row is removed, since only internal nucleon interactions are being examined. With that, the N-body system can be transformed into an $(N-1)$-body system by discarding the center-of-mass coordinates.

With the coordinate transformation $\boldsymbol{r} \to J\boldsymbol{r} = \boldsymbol{r}'$ established, extraction vectors are introduced to isolate specific coordinates in both physical and momentum space. These are denoted w_i for physical space and u_i for momentum space. They are unit vectors with 1 in the i'th slot. Under a coordinate transformation they transform as $w_i \to U^{\mathsf{T}} w_i$, where $U = J^{-1}$, since

$$w^{\mathsf{T}}\boldsymbol{r} \to w^{\mathsf{T}} J^{-1} J\boldsymbol{r} = (U^{\mathsf{T}} w)^{\mathsf{T}} \boldsymbol{r}'. \tag{8}$$

For momentum space, the transformation is different, $u_i \to J u_i$ since $u^{\mathsf{T}}\boldsymbol{k} = -i \sum_i u_i \frac{\partial}{\partial r_i}$, which shows

$$u^{\mathsf{T}}\boldsymbol{k} = -i \sum_i u_i \frac{\partial}{\partial r_i} = -i \sum_i u_i \frac{\partial}{\partial r'_j} \frac{\partial r'_j}{\partial r_i} = u_i J_{ij} k'_j = (Ju)^{\mathsf{T}} \boldsymbol{k}'. \tag{9}$$

For the $pn\pi$ system with particle ordering (p, n, π), the full explicit Jacobi matrix is

$$J_3 = \begin{pmatrix} \frac{m_p}{m_p} & -1 & 0 \\ \frac{m_p}{m_p+m_n} & \frac{m_n}{m_p+m_n} & -1 \\ \frac{m_p}{m_p+m_n+m_\pi} & \frac{m_n}{m_p+m_n+m_\pi} & \frac{m_\pi}{m_p+m_n+m_\pi} \end{pmatrix},$$

where the last row can be removed and the matrix rewritten in terms of reduced masses.

$$J_{pn\pi} = \begin{pmatrix} 1 & -1 & 0 \\ \frac{m_p}{m_p+m_n} & \frac{m_n}{m_p+m_n} & -1 \end{pmatrix},$$

The modified matrix $J_{pn\pi}$ is then used to express the three-body wavefunction purely in terms of the two relative coordinates, discarding the center-of-mass coordinate:

$$J_{pn\pi} \begin{pmatrix} \boldsymbol{r_p} \\ \boldsymbol{r_n} \\ \boldsymbol{r_\pi} \end{pmatrix} = \begin{pmatrix} \boldsymbol{r}_p - \boldsymbol{r}_n \\ \frac{m_p \boldsymbol{r}_p + m_n \boldsymbol{r}_n}{m_p+m_n} - \boldsymbol{r}_\pi \end{pmatrix} = \begin{pmatrix} \boldsymbol{r}_{pn} \\ \boldsymbol{r}_{pn\pi} \end{pmatrix}. \tag{10}$$

This shows that $\boldsymbol{r}_{pn}$ is the separation between proton and neutron, and $\boldsymbol{r}_{pn\pi}$ is the distance from the pion to the center of mass of the nucleon pair. In practice, this means that the kinetic energy splits into relative motions with reduced masses, e.g., μ_{np} for the pn coordinate and $\mu_{np\pi}$ for the pion relative to the pn pair.

4 | Correlated Shifted Gaussian

To model the spatial wavefunction, the Gaussian method is used, where the wavefunction is built as a linear combination of correlated shifted Gaussians. The correlated Gaussian is defined as [2]

$$\exp\left(-\sum_{i,j=1}^{N} A_{i,j} \boldsymbol{r}_i \cdot \boldsymbol{r_j}\right) \equiv e^{-\boldsymbol{r}^\mathsf{T} A \boldsymbol{r}}, \tag{11}$$

which defines a system of N particles where $\boldsymbol{r} = (\boldsymbol{r}_1, ..., \boldsymbol{r}_N)$ is a N-dimensional column vector of 3-dimensional particle coordinate vectors $\boldsymbol{r}_j$, with unit length fm (fermi), for particle j. The matrix A is a $N \times N$ symmetric positive-definite particle correlation matrix with units fm^{-2}. To allow the basis to describe states with non-zero orbital angular momentum and break spherical symmetry, a spatial shift $\boldsymbol{r}_0$ is introduced to the coordinate vector,

$$\exp\left(-(\boldsymbol{r} - \boldsymbol{r}_0)^\mathsf{T} A (\boldsymbol{r} - \boldsymbol{r}_0)\right) = \exp\left(-\boldsymbol{r}^\mathsf{T} A \boldsymbol{r} + 2\boldsymbol{r}_0{}^\mathsf{T} A \boldsymbol{r} - \boldsymbol{r}_0{}^\mathsf{T} A \boldsymbol{r}_0\right), \tag{12}$$

the last part is a constant and is therefore omitted. Defining $\boldsymbol{s}^\mathsf{T} = \frac{1}{2}\boldsymbol{r}_0{}^\mathsf{T} A$ yields the final correlated shifted Gaussian:

$$e^{-\boldsymbol{r}^\mathsf{T} A \boldsymbol{r} + \boldsymbol{s}^\mathsf{T} \boldsymbol{r}} = \exp\left(-\sum_{i,j=1}^{N} A_{i,j} \boldsymbol{r}_i \cdot \boldsymbol{r}_{\boldsymbol{j}} + \sum_{i=1}^{N} \boldsymbol{s}_i \cdot \boldsymbol{r}_i \right) = \langle \boldsymbol{r} \,|\, g \rangle. \tag{13}$$

Each basis function is determined by two parameters: the matrix A and the shift $\boldsymbol{s}$. This makes the Gaussian basis computationally efficient for calculating all necessary matrix elements.

4.1 Overlap

Since the product of two Gaussians is again a Gaussian, the overlap integral between two shifted correlated Gaussians reduces to a single Gaussian integral with an effective matrix $B = A + A'$ and effective shift $\boldsymbol{v} = \boldsymbol{s} + \boldsymbol{s}'$. The matrix B is diagonalized with an orthogonal matrix Q so that $B = QDQ^\mathsf{T}$, and coordinates are transformed as $\boldsymbol{r} = Q\boldsymbol{x}$. This decouples the integral into a product of N independent 3D Gaussian integrals [2].

$$\begin{aligned}
\langle g' \,|\, g \rangle &= \int d^3\boldsymbol{r}_N \, e^{-\boldsymbol{r}^\mathsf{T} B \boldsymbol{r} + \boldsymbol{v}^\mathsf{T} \boldsymbol{r}}, \\
&= \prod_{i=1}^{N} \int d^3\boldsymbol{x}_i \, e^{-\boldsymbol{x}_i \cdot D_{ii} \boldsymbol{x}_i + \boldsymbol{v}_i \cdot \boldsymbol{x}_i}, \\
&= \prod_{i=1}^{N} e^{\frac{1}{4D_{ii}} \boldsymbol{v}_i^2} \left(\frac{\pi}{D_{ii}} \right)^{3/2}, \\
&= \left(\frac{\pi^N}{\det B} \right) e^{\frac{1}{4} \boldsymbol{v}^\mathsf{T} B^{-1} \boldsymbol{v}} \equiv M.
\end{aligned} \tag{14}$$

This yields the unnormalized overlap element M, which is subsequently normalized when solving the generalized eigenvalue problem.

The Gaussians can be used to evaluate functions of the form $\langle g'|f(w^{\mathsf{T}}\boldsymbol{r})|g\rangle$, such as $w^{\mathsf{T}}\boldsymbol{r}$ and $(w^{\mathsf{T}}\boldsymbol{r})^2$. Differentiating the exponential with respect to the shift, pulls down coordinate factors $\boldsymbol{r}$.

$$\begin{aligned}\langle g'|w^{\mathsf{T}}\boldsymbol{r}|g\rangle &= \int d^3\boldsymbol{r}\; w^{\mathsf{T}}\boldsymbol{r}e^{-\boldsymbol{r}^{\mathsf{T}}B\boldsymbol{r}+\boldsymbol{v}^{\mathsf{T}}\boldsymbol{r}},\\ &= w^{\mathsf{T}}\nabla_{\boldsymbol{v}}\int d^3\boldsymbol{r}e^{-\boldsymbol{r}^{\mathsf{T}}B\boldsymbol{r}+\boldsymbol{v}^{\mathsf{T}}\boldsymbol{r}},\\ &= w^{\mathsf{T}}\left(\frac{\partial}{\partial\boldsymbol{v}^{\mathsf{T}}}\right)e^{\frac{1}{4}\boldsymbol{v}^{\mathsf{T}}B^{-1}\boldsymbol{v}}\left(\frac{\pi^N}{\det B}\right)^{3/2} = w^{\mathsf{T}}\boldsymbol{u}M, \qquad (15)\end{aligned}$$

where $\boldsymbol{u} = \frac{1}{2}B^{-1}\boldsymbol{v}$. Expressing the result in terms of $\boldsymbol{u}$ isolates the dependence on the spatial shifts, simplifying the algebraic evaluation of higher-order matrix elements. For $(w^{\mathsf{T}}\boldsymbol{r})^2$ the derivation is similar and yields:

$$\begin{aligned}\langle g'|\boldsymbol{r}^{\mathsf{T}}ww^{\mathsf{T}}\boldsymbol{r}|g\rangle &= \left(\frac{\partial}{\partial\boldsymbol{v}}ww^{\mathsf{T}}\frac{\partial}{\partial\boldsymbol{v}^{\mathsf{T}}}\right)M,\\ &= \left[\frac{3}{2}w^{\mathsf{T}}B^{-1}w + \frac{1}{4}\left(w^{\mathsf{T}}B^{-1}\boldsymbol{v}\right)\left(\boldsymbol{v}^{\mathsf{T}}B^{-1}w\right)\right]M,\\ &= \left(\frac{3}{2}w^{\mathsf{T}}B^{-1}w + \boldsymbol{u}^{\mathsf{T}}ww^{\mathsf{T}}\boldsymbol{u}\right)M. \qquad (16)\end{aligned}$$

The formula holds for any smooth function of $w^{\mathsf{T}}\boldsymbol{r}$. By expressing $f(w^{\mathsf{T}}\boldsymbol{r})$ through its Fourier transform $\mathcal{F}(\boldsymbol{k})$, the operator can be evaluated as an exponential applied to the Gaussian states. This yields a momentum-space integral:

$$\langle g'|f(w^{\mathsf{T}}\boldsymbol{r})|g\rangle = M\int\frac{d^3\boldsymbol{k}}{(2\pi)^3}\mathcal{F}(\boldsymbol{k})e^{-\alpha k^2+i\boldsymbol{k}\cdot\boldsymbol{q}}, \qquad (17)$$

where $\alpha = \frac{1}{4}w^{\mathsf{T}}B^{-1}w$ and $\boldsymbol{q} = w^{\mathsf{T}}\boldsymbol{u}$.

Introducing the substitution $\beta = \frac{1}{4\alpha} = (w^{\mathsf{T}}B^{-1}w)^{-1}$ allows this expression to be transformed back into coordinate space as a 3D integral weighted by a displaced Gaussian, $e^{-\beta(\boldsymbol{r}-\boldsymbol{q})^2}$. Analytically integrating the angular components of this displaced Gaussian generates a spherical sine function.

This successfully reduces the complex 3D problem into a closed-form 1D radial integral [2]:

$$\langle g'|f(|w^{\mathsf{T}}\boldsymbol{r}|)|g\rangle = M\left(\frac{\beta}{\pi}\right)^{\frac{3}{2}} 2\pi\frac{e^{-\beta q^2}}{\beta q}\int_0^\infty r dr f(r) e^{-\beta r^2}\sinh\left(2\beta q r\right), \quad (18)$$

where $q = |\boldsymbol{q}|$. These variables are essential for calculating the kinetic energy in Section 4.3.

4.2 Momentum Space

To efficiently calculate the kinetic energy, the basis functions are evaluated in momentum space using a Fourier transform. The convention $\langle \boldsymbol{r} \,|\, \boldsymbol{k}\rangle = e^{i\boldsymbol{k}^{\mathsf{T}}\boldsymbol{r}}$ is adopted alongside the corresponding completeness relation $\int \frac{d^{3N}\boldsymbol{k}}{(2\pi)^{3N}} |\boldsymbol{k}\rangle\langle\boldsymbol{k}| = 1$. This specific choice systematically handles the $(2\pi)^{3N}$ factors in all subsequent matrix elements and ensures that normalization is preserved between coordinate and momentum space.

Because the spatial wavefunction is Gaussian, its Fourier transform remains Gaussian in $\boldsymbol{k}$, with a transformed width matrix and a complex shift. By inserting a spatial completeness relation, the inner product becomes an integral over the configuration space:

$$\begin{aligned}
\langle \boldsymbol{k} \,|\, g\rangle &= \int d^{3N}\boldsymbol{r}\, e^{-i\boldsymbol{k}^{\mathsf{T}}\boldsymbol{r}} e^{-\boldsymbol{r}^{\mathsf{T}}A\boldsymbol{r}+\boldsymbol{s}^{\mathsf{T}}\boldsymbol{r}}, \\
&= \left(\frac{\pi^N}{\det(A)}\right)^{3/2} e^{\frac{1}{4}(\boldsymbol{s}-i\boldsymbol{k})^{\mathsf{T}}A^{-1}(\boldsymbol{s}-i\boldsymbol{k})}, \\
&= \left(\frac{\pi^N}{\det(A)}\right)^{3/2} e^{\frac{1}{4}\boldsymbol{s}^{\mathsf{T}}A^{-1}\boldsymbol{s}} \cdot e^{-\frac{1}{4}\boldsymbol{k}^{\mathsf{T}}A^{-1}\boldsymbol{k}} \cdot e^{-\frac{1}{2}i\boldsymbol{k}^{\mathsf{T}}A^{-1}\boldsymbol{s}}, \qquad (19)
\end{aligned}$$

which isolates the momentum-dependent variables into a new Fouriertransformed Gaussian state:

$$|\tilde{g}\rangle = e^{-\boldsymbol{k}^{\mathsf{T}}\tilde{A}\boldsymbol{k}+\tilde{\boldsymbol{s}}^{\mathsf{T}}\boldsymbol{k}}, \qquad (20)$$

where the transformed width matrix is $\tilde{A} = \frac{1}{4}A^{-1}$ and the complex momentum shift is $\tilde{\boldsymbol{s}} = \frac{-i}{2}A^{-1}\boldsymbol{s}$.

The factor $\mathcal{M}(A, \boldsymbol{s})$ collects the A- and $\boldsymbol{s}$-dependent prefactors, so that the remaining $|\tilde{g}\rangle$ has the same Gaussian form as in coordinate space but expressed in momentum variables:

$$\mathcal{M}(A, \boldsymbol{s}) = \left(\frac{\pi^N}{\det(A)}\right)^{3/2} e^{\frac{1}{4}\boldsymbol{s}^\mathsf{T} A^{-1}\boldsymbol{s}}, \tag{21}$$

giving the final solution

$$\langle \boldsymbol{k} \,|\, g\rangle = \mathcal{M}(A, \boldsymbol{s})|\tilde{g}\rangle. \tag{22}$$

Because the functions retain their Gaussian properties, the overlap in momentum space can be calculated using the same framework as the spatial overlap:

$$\begin{aligned}
\langle g' \,|\, g\rangle &= \int \frac{d^{3N}\boldsymbol{k}}{(2\pi)^{3N}} \langle g' \,|\, \boldsymbol{k}\rangle\langle \boldsymbol{k} \,|\, g\rangle, \\
&= \left(\frac{\pi^N}{\det A'}\frac{\pi^N}{\det A}\right)^{3/2} \frac{e^{\frac{1}{4}\boldsymbol{s}'^\top A'^{-1}\boldsymbol{s}'} e^{\frac{1}{4}\boldsymbol{s}^\mathsf{T} A^{-1}\boldsymbol{s}}}{(2\pi)^{3N}} \langle \tilde{g}' \,|\, \tilde{g}\rangle, \\
&= \mathcal{M}(A', \boldsymbol{s}')\mathcal{M}(A, \boldsymbol{s}) \frac{\langle \tilde{g}' \,|\, \tilde{g}\rangle}{(2\pi)^{3N}}.
\end{aligned} \tag{23}$$

This factorization enables the efficient computation of kinetic energy as integrals over momentum, as detailed in the next section.

4.3 Kinetic Energy

The overlap can now be used to calculate the matrix element for the general momentum operator $f(u^\mathsf{T}\boldsymbol{k})$. By inserting a momentum-space completeness relation and evaluating the resulting Gaussian integral, the matrix element is reduced to a radial integral over $x = |\boldsymbol{k}|$, which depends only on the scalar $u^\mathsf{T}\boldsymbol{k}$.

$$\begin{aligned}
\langle g'|f(|u^\mathsf{T}\boldsymbol{k}|)|g\rangle &= \int \frac{d^{3N}\boldsymbol{k}}{(2\pi)^{3N}} \langle g' \,|\, \boldsymbol{k}\rangle f(|u^\mathsf{T}\boldsymbol{k}|)\langle \boldsymbol{k} \,|\, g\rangle, \\
&= \mathcal{M}(A', \boldsymbol{s}')\mathcal{M}(A, \boldsymbol{s}) \frac{1}{(2\pi)^{3N}} \langle \tilde{g}'|f(|u^\mathsf{T}\boldsymbol{x}|)|\tilde{g}\rangle,
\end{aligned} \tag{24}$$

To evaluate this, the closed-form integration from equation (18) is used:

$$\begin{aligned}\langle g'|f(|u^\mathsf{T}\boldsymbol{k}|)|g\rangle &= \mathcal{M}(A',\boldsymbol{s}')\mathcal{M}(A,\boldsymbol{s})\frac{\langle\tilde{g}'\,|\,\tilde{g}\rangle}{(2\pi)^{3N}}\left(\frac{\gamma}{\pi}\right)^{3/2}\\ &\quad\times 2\pi\frac{e^{-\gamma(i\eta)^2}}{i\gamma\eta}\int_0^\infty dx x\tilde{f}(x)e^{-\gamma x^2}\sinh(2i\gamma\eta x),\\ &= \langle g'\,|\,g\rangle\left(\frac{\gamma}{\pi}\right)^{3/2}2\pi\frac{e^{\gamma\eta^2}}{\gamma\eta}\int_0^\infty dx x\tilde{f}(x)e^{-\gamma x^2}\sin(2\gamma\eta x),\end{aligned} \tag{25}$$

where the parameter γ controls the effective width of the Gaussian in momentum space, while $\boldsymbol{\eta}$ encodes the shift dependence,

$$\frac{1}{\gamma} = u^\mathsf{T}\tilde{R}u = u^\mathsf{T}\left(\tilde{A}+\tilde{A}'\right)^{-1}u = 4u^\mathsf{T}\left(A^{-1}+A'^{-1}\right)^{-1}u = 4u^\mathsf{T}ARA'u, \tag{26}$$

where R is defined as $R = B^{-1} = (A+A')^{-1}$. The shift component is given by:

$$\boldsymbol{\eta} = u^\mathsf{T}\left(AR\boldsymbol{s}' - A'R\boldsymbol{s}\right), \tag{27}$$

For unshifted Gaussians ($\boldsymbol{\eta}\to 0$), the expression simplifies since:

$$\lim_{\eta\to 0}\frac{e^{\gamma\eta^2}}{\gamma\eta}\sin(2\gamma\eta x) = 2x, \tag{28}$$

and the remaining integral becomes a standard Gaussian moment, yielding the closed-form expression:

$$\langle g'|f(|u^\mathsf{T}\boldsymbol{k}|)|g\rangle = \left(\frac{\pi^N}{\det B}\right)4\pi\left(\frac{\gamma}{\pi}\right)^{3/2}\int_0^\infty dx x^2\tilde{f}(x)e^{-\gamma x^2}. \tag{29}$$

With a general form for the momentum function established, the non-relativistic kinetic energy function can be used:

$$\tilde{f}(u^\mathsf{T}\boldsymbol{k}) = \frac{(u^\mathsf{T}\boldsymbol{k})^2}{2m}. \tag{30}$$

Evaluating the integral against the Gaussian weight produces the analytical shifted matrix element:

$$\begin{aligned}\langle g'|\frac{(u^{\mathsf{T}}\boldsymbol{k})^2}{2m}|g\rangle &= \langle g'\,|\,g\rangle\frac{2\pi}{2m}\left(\frac{\gamma}{\pi}\right)^{3/2}\frac{e^{\gamma\eta^2}}{\gamma\eta}\int_0^\infty dx x^3 e^{-\gamma x^2}\sin(2\gamma\eta x),\\ &= \langle g'\,|\,g\rangle\frac{2\pi}{2m}\left(\frac{\gamma}{\pi}\right)^{3/2}\frac{e^{\gamma\eta^2}}{\gamma\eta}\frac{\sqrt{\pi}e^{-\gamma\eta^2}}{4\gamma^{3/2}}\left(3\eta-2\gamma\eta^3\right),\\ &= \frac{\langle g'\,|\,g\rangle}{2m}\left(\frac{3}{2}\frac{1}{\gamma}-\eta^2\right).\end{aligned} \tag{31}$$

In the case where there is no shift of the gaussians, it simplifies to:

$$\begin{aligned}\langle g'|\frac{(u^{\mathsf{T}}\boldsymbol{k})^2}{2m}|g\rangle &= \langle g'\,|\,g\rangle\left(\frac{\gamma}{\pi}\right)^{3/2}\frac{4\pi}{2m}\int_0^\infty dx x^4 e^{-\gamma x^2},\\ &= \langle g'\,|\,g\rangle\frac{4\pi}{2m}\left(\frac{\gamma}{\pi}\right)^{3/2}\frac{3\sqrt{\pi}}{8\gamma^{5/2}} = \langle g'\,|\,g\rangle\frac{3}{m}(u^{\mathsf{T}}A'RAu).\end{aligned} \tag{32}$$

To include relativistic corrections, the non-relativistic kinetic energy $p^2/2m$ is replaced with the exact relativistic form $\sqrt{p^2+m^2}-m$, keeping the same momentum-space framework, but using the function

$$\tilde{f}(u^{\mathsf{T}}\boldsymbol{k}) = \sqrt{(u^{\mathsf{T}}\boldsymbol{k})^2+m^2}-m, \tag{33}$$

yields the relativistic shifted matrix element:

$$\begin{aligned}&\langle g'|\left(\sqrt{(u^{\mathsf{T}}\boldsymbol{k})^2+m^2}-m\right)|g\rangle\\ &= \langle g'\,|\,g\rangle\left(\frac{\gamma}{\pi}\right)^{3/2}2\pi\frac{e^{\gamma\eta^2}}{\gamma\eta}\int_0^\infty dx x e^{-\gamma x^2}\sin(2\gamma\eta x)\left(\sqrt{x^2+m^2}-m\right),\end{aligned} \tag{34}$$

which again simplifies for unshifted gaussians ($\boldsymbol{\eta}=0$) to:

$$\begin{aligned}&\langle g'|\left(\sqrt{(u^{\mathsf{T}}\boldsymbol{k})^2+m^2}-m\right)|g\rangle\\ &= \langle g'\,|\,g\rangle\left(\frac{\gamma}{\pi}\right)^{3/2}4\pi\int_0^\infty dx x^2 e^{-\gamma x^2}\left(\sqrt{x^2+m^2}-m\right).\end{aligned} \tag{35}$$

Unlike the classical operator, these relativistic integrals cannot be solved analytically and must be evaluated numerically using Simpson's rule. Because the analytical integral limits extend from zero to infinity, the numerical integration requires a carefully chosen upper momentum cutoff.

Furthermore, because the system is transformed into Jacobi coordinates, to remove the center of mass, the mass parameter m in these equations explicitly represents the reduced mass μ of the specific relative subsystem being evaluated.

Finally, it can be verified that in the low momentum regime ($x \ll m$), the relativistic energy converges to the classical energy, as the operator can be expanded using a Taylor approximation:

$$\begin{aligned}\sqrt{x^2+m^2} - m &= m\left(\sqrt{1+\left(\frac{x}{m}\right)^2} - 1\right) \\ &\approx m\left(1 + \frac{x^2}{2m^2} - 1\right) = \frac{x^2}{2m}. \end{aligned} \tag{36}$$

Substituting this approximation back into the full integral yields:

$$\begin{aligned}\langle g'|T_{\text{rel}}|g\rangle &\approx \langle g' \,|\, g\rangle \left(\frac{\gamma}{\pi}\right)^{3/2} 2\pi \frac{e^{\gamma\eta^2}}{\gamma\eta} \int_0^\infty dx\, x e^{-\gamma x^2} \sin(2\gamma\eta x) \left(\frac{x^2}{2m}\right) \\ &= \langle g' \,|\, g\rangle \frac{2\pi}{2m} \left(\frac{\gamma}{\pi}\right)^{3/2} \frac{e^{\gamma\eta^2}}{\gamma\eta} \int_0^\infty dx\, x^3 e^{-\gamma x^2} \sin(2\gamma\eta x). \end{aligned} \tag{37}$$

This confirms that the numerical relativistic integral recovers the analytical classical integral for heavy non-relativistic particles.

4.4 Charge Radius

Physical observables can be extracted directly from the overlap formulas. One key quantity is the charge radius, which measures the spatial extent of the charge distribution in the deuteron. Physically, this radius is not determined solely by the proton's position, it is also modified by the intrinsic charge distribution of the neutron and the spatial extent of the charged virtual pions (π^+ and π^-) that mediate the strong interaction.

This macroscopic radius is computed using the expectation value of r^2 within the Gaussian basis, allowing the model parameters to be fitted to match the experimental value.

$$r_d = \sqrt{\langle r_c^2 \rangle + r_p^2 + r_n^2}, \tag{38}$$

$$\langle r_c^2 \rangle = \frac{u^\mathsf{T} R^2 c}{c^\mathsf{T} \mathcal{N} c}, \tag{39}$$

$$R_{ij}^2 = \langle \psi_i | \boldsymbol{r}^\mathsf{T} w w^\mathsf{T} \boldsymbol{r} | \psi_j \rangle, \tag{40}$$

where r_d is the total charge radius, r_c is the RMS radius of the charge distribution in the center-of-mass frame. The intrinsic squared radii of proton and neutron are $r_p^2 \approx 0.708\,\mathrm{fm}^2$ and $r_n^2 \approx -0.1161\,\mathrm{fm}^2$. The second line demonstrates how r_c^2 is extracted from the matrix element R^2 using the optimized basis coefficients c. The charge radius can be used to fit parameters later, as it has an experimentally well-defined value for the deuteron.

5 | Pion-Nucleon Coupling

5.1 The Bare Deuteron state

Before the deuteron nucleus emits a pion, it is in a so-called bare state. In this state there is only one proton and one neutron with total spin $S = 1$, isospin $I = 0$ and parity $+1$. The proton and neutron are both fermions, so their final wavefunction must be antisymmetrical. The spin wavefunction forms a spin triplet, allowing for the selection of a reference frame where $\chi = |\uparrow\uparrow\rangle$. The isospin wavefunction is a singlet and therefore antisymmetric $\xi = \frac{1}{\sqrt{2}} (|pn\rangle - |np\rangle)$. To get a final antisymmetric wavefunction, the spatial wavefunction must be symmetric, but our standard shifted Gaussian is not symmetric under particle exchange:

$$P_{12}|A, s\rangle = e^{-(-\boldsymbol{r})^\mathsf{T} A(-\boldsymbol{r}) + \boldsymbol{s}^\mathsf{T}(-\boldsymbol{r})} = e^{-\boldsymbol{r}^\mathsf{T} A \boldsymbol{r} - \boldsymbol{s}^\mathsf{T} \boldsymbol{r}}, \tag{41}$$

To construct a symmetric spatial wavefunction, a linear combination is used:

$$\psi = |A, s\rangle + |A, -s\rangle. \tag{42}$$

The spatial wavefunction is not explicitly normalized, since the two Gaussians are not orthogonal. Any spatial normalization constants are absorbed into the c_i coefficients when solving the generalized eigenvalue problem.

Combining the isospin, spin, and spatial components, yields the final wavefunction for the bare deuteron state:

$$\begin{aligned} |\Psi_{pn}\rangle &= |\xi\rangle \otimes |\chi\rangle \otimes |\psi\rangle \\ &= \frac{1}{\sqrt{2}} \left(|pn\rangle - |np\rangle\right) |\uparrow\uparrow\rangle \left(|A, a\rangle + |A, -a\rangle\right). \end{aligned} \tag{43}$$

By applying the coupling operator W to the bare pn state, a superposition of one-pion intermediate states is generated. Each resulting state must preserve the global quantum numbers: total isospin $I = 0$, total spin $S = 1$, and positive parity $+1$. These constraints limit the accessible channels and determine the structure of the Hamiltonian matrix in equation (2).

5.2 Pions

The pion is a meson with 3 charge states $\{\pi^0, \pi^-, \pi^+\}$. Therefore the pion is an isospin-vector with total isospin $I = 1$, it has spin $S = 0$ and parity -1. When the W coupling operator acts, it must change these quantum numbers in a way that conserves total isospin $I = 0$, total spin $S = 1$, and total parity $+1$ of the system.

5.3 The Total Coupling Operator

In the nuclear model with explicit mesons, an exchange operator is used to simulate the nucleons emitting and absorbing pions. Since both nucleons in this system can exchange pions, the total pion-nucleon coupling operator is the sum of the individual one-body emission operators for the proton and the neutron:

$$\begin{aligned} W &= W_1 + W_2 \\ &= (\boldsymbol{\tau}_1 \cdot \boldsymbol{\pi})(\boldsymbol{\sigma}_1 \cdot {w_{\pi 1}}^{\mathsf{T}} \boldsymbol{r}) f({w_{\pi 1}}^{\mathsf{T}} \boldsymbol{r}) + (\boldsymbol{\tau}_2 \cdot \boldsymbol{\pi})(\boldsymbol{\sigma}_2 \cdot {w_{\pi 2}}^{\mathsf{T}} \boldsymbol{r}) f({w_{\pi 2}}^{\mathsf{T}} \boldsymbol{r}). \end{aligned} \tag{44}$$

Here, $\boldsymbol{\tau}$ and $\boldsymbol{\sigma}$ are the isospin- and spin Pauli matrices, $\boldsymbol{\pi}$ is the pion isospin-vector, and ${w_{\pi i}}^{\mathsf{T}}\boldsymbol{r}$ is the distance from the emitted pion to the emitting nucleon i.

The function $f({w_{\pi i}}^{\mathsf{T}}\boldsymbol{r})$ represents an effective short-range form factor, which ensures the interaction occurs only when the particles are in close proximity and that the total parity is satisfied. To allow for analytic evaluation within the Correlated Gaussian method, this form factor is modeled as a Gaussian function:

$$f({w_{\pi i}}^{\mathsf{T}}\boldsymbol{r}) = \frac{S}{b_\pi}\exp\left(-\frac{\boldsymbol{r}^{\mathsf{T}}w_{\pi i}{w_{\pi i}}^{\mathsf{T}}\boldsymbol{r}}{b_\pi^2}\right)\exp\left(-\frac{\boldsymbol{r}^{\mathsf{T}}w_{NN}{w_{NN}}^{\mathsf{T}}\boldsymbol{r}}{b_N^2}\right), \tag{45}$$

where S determines the strength of the coupling (with units of MeV), b_π and b_N dictates the interaction range. The first exponent controls the interaction range for the emitted pion, by limiting the distance it can have to the emitting nucleon i. The second exponent limits the distance between the nucleons, forcing them to stay in close proximity, to mimic a bound state. This Gaussian form factor, is a practical approximation chosen for computational convenience. A more realistic form would derive from letting the nucleons exchange pions, no matter their separation, and then find the binding energy as the difference between the ground state and the first exited state energy. This approach was tested, but finding convergence and consistent bound states proved difficult, therefore the simple Gaussian form factor was used instead.

5.4 Isospin Space

The isospin operator determines the charge of the emitted pion and the resulting nucleon states. The isospin interaction is given by:

$$(\boldsymbol{\tau}\cdot\boldsymbol{\pi}) = \tau^0\pi^0 + \sqrt{2}\tau^-\pi^+ + \sqrt{2}\tau^+\pi^-, \tag{46}$$

where the isospin Pauli matrices are:

$$\tau^0 = \begin{pmatrix}1 & 0\\ 0 & -1\end{pmatrix}, \quad \tau^- = \begin{pmatrix}0 & 0\\ 1 & 0\end{pmatrix}, \quad \tau^+ = \begin{pmatrix}0 & 1\\ 0 & 0\end{pmatrix}, \tag{47}$$

so that $\tau^+|n\rangle = |p\rangle$ and $\tau^-|p\rangle = |n\rangle$, which fixes the overall sign of the charged-pion channels.

This creates four possible interactions when $(\boldsymbol{\tau} \cdot \boldsymbol{\pi})$ interacts with a nucleon, and their corresponding coefficients:

$$\langle \pi^0 p | (\boldsymbol{\tau} \cdot \boldsymbol{\pi}) | p \rangle = +1, \tag{48}$$

$$\langle \pi^+ n | (\boldsymbol{\tau} \cdot \boldsymbol{\pi}) | p \rangle = \sqrt{2}, \tag{49}$$

$$\langle \pi^0 n | (\boldsymbol{\tau} \cdot \boldsymbol{\pi}) | n \rangle = -1, \tag{50}$$

$$\langle \pi^- p | (\boldsymbol{\tau} \cdot \boldsymbol{\pi}) | n \rangle = \sqrt{2}. \tag{51}$$

These four matrix elements show how isospin conservation constrains the pion emission process. The factors reflect Clebsch-Gordan coefficients when coupling the pion's isospin to the nucleon pair.

5.5 Spin and Spatial Space

An initial configuration is defined, where both nucleons have parallel spins, the spin-triplet state $|\uparrow\uparrow\rangle$. Using spin interaction coordinates $(\boldsymbol{\sigma} \cdot \boldsymbol{r})$ consisting of the Pauli spin matrices. The spin operator $\boldsymbol{\sigma}$ and the position components are both expressed in the spherical tensor basis to ensure proper angular momentum coupling:

$$\sigma^0 = \begin{pmatrix} 1 & 0 \\ 0 & -1 \end{pmatrix}, \quad \sigma^- = \begin{pmatrix} 0 & 0 \\ 1 & 0 \end{pmatrix}, \quad \sigma^+ = \begin{pmatrix} 0 & 1 \\ 0 & 0 \end{pmatrix}, \tag{52}$$

and the position vector consists of:

$$r^0 = z, \quad r^+ = \frac{x + iy}{\sqrt{2}}, \quad r^- = \frac{x - iy}{\sqrt{2}}. \tag{53}$$

Here $(r^0, r^\pm)$ are the spherical components of $\boldsymbol{r}$, and the spin operators $\sigma^0, \sigma^\pm$ are written in the same spherical basis so that $(\boldsymbol{\sigma} \cdot \boldsymbol{r}) = \sigma^0 r^0 + \sqrt{2}\sigma^- r^+ + \sqrt{2}\sigma^+ r^-$. Like the isospin part, there are also 4 contributions from the spin interaction:

$$\langle \uparrow | (\boldsymbol{\sigma} \cdot \boldsymbol{r}) | \uparrow \rangle = +r^0, \tag{54}$$

$$\langle \downarrow | (\boldsymbol{\sigma} \cdot \boldsymbol{r}) | \uparrow \rangle = \sqrt{2} r^+, \tag{55}$$

$$\langle \uparrow | (\boldsymbol{\sigma} \cdot \boldsymbol{r}) | \downarrow \rangle = \sqrt{2} r^-, \tag{56}$$

$$\langle \downarrow | (\boldsymbol{\sigma} \cdot \boldsymbol{r}) | \downarrow \rangle = -r^0, \tag{57}$$

but since a system is chosen where the bare state only consists of spin-up, the two last will not be used.

5.6 Matrix Elements

With the spin and isospin matrices fully defined, all the possible states can be constructed. This is done by applying equation (44) to the full wavefunction of the pn state. This is a long derivation, which can be seen in appendix A.

As an example, the neutral pion channel (π^0) will be evaluated, the deviation is similar for the other pions. Isolating the (τ^0) component shows the resulting isospin function:

$$\tau_1^0 \frac{1}{\sqrt{2}} \left(|pn\rangle - |np\rangle\right) = +\frac{1}{\sqrt{2}} \left(|pn\rangle + |np\rangle\right), \tag{58}$$

$$\tau_2^0 \frac{1}{\sqrt{2}} \left(|pn\rangle - |np\rangle\right) = -\frac{1}{\sqrt{2}} \left(|pn\rangle + |np\rangle\right). \tag{59}$$

The negative sign is absorbed into the calculations of the spin part, and the resulting isospin wavefunction becomes symmetric: $|\xi_{\pi^0}\rangle = \frac{1}{\sqrt{2}} \left(|pn\rangle + |np\rangle\right)$. The spin part becomes antisymmetric and the negative factor from the isospin wavefunction is inserted to get:

$$\begin{aligned} W_{\pi^0}|\chi\rangle &= \left[(\boldsymbol{\sigma}_1 \cdot {w_{\pi 1}}^{\mathsf{T}}\boldsymbol{r}) f({w_{\pi 1}}^{\mathsf{T}}\boldsymbol{r}) - (\boldsymbol{\sigma}_2 \cdot {w_{\pi 2}}^{\mathsf{T}}\boldsymbol{r}) f({w_{\pi 2}}^{\mathsf{T}}\boldsymbol{r})\right] |\uparrow\uparrow\rangle, \\ &= f({w_{\pi 1}}^{\mathsf{T}}\boldsymbol{r}) \left[{w_{\pi 1}}^{\mathsf{T}} r^0 |\uparrow\uparrow\rangle + \sqrt{2} {w_{\pi 1}}^{\mathsf{T}} r^+ |\downarrow\uparrow\rangle\right] \\ &\quad - f({w_{\pi 2}}^{\mathsf{T}}\boldsymbol{r}) \left[{w_{\pi 2}}^{\mathsf{T}} r^0 |\uparrow\uparrow\rangle + \sqrt{2} {w_{\pi 2}}^{\mathsf{T}} r^+ |\uparrow\downarrow\rangle\right] \end{aligned} \tag{60}$$

This structure highlights that the spatial form factor $f(w^{\mathsf{T}}\boldsymbol{r})$ binds closely to the coordinates of the specific emitting nucleon, driving transitions between parallel and antiparallel spin configurations. This breaks down into three distinct geometric possibilities:

- There is no flip in spin, $f({w_{\pi 1}}^{\mathsf{T}}\boldsymbol{r}) {w_{\pi 1}}^{\mathsf{T}} r^0 - f({w_{\pi 2}}^{\mathsf{T}}\boldsymbol{r}) {w_{\pi 2}}^{\mathsf{T}} r^0$.
- The spin of the first nucleon is flipped, $f({w_{\pi 1}}^{\mathsf{T}}\boldsymbol{r}) \sqrt{2} {w_{\pi 1}}^{\mathsf{T}} r^+$.
- The spin of the second nucleon is flipped, $-f({w_{\pi 2}}^{\mathsf{T}}\boldsymbol{r}) \sqrt{2} {w_{\pi 2}}^{\mathsf{T}} r^+$.

Each spatial form $(w_i^T r^0, w_i^T r^+, w_i^T r^-)$ couples to different Gaussian overlaps, because they have different $\boldsymbol{r}$ dependence. The Hamiltonian matrix therefore treats each as an independent basis state with its own matrix element, giving 3×3 pion channels (3 pion types times 3 spin couplings).

Before completing the state assembly, parity conservation must be satisfied. The deuteron ground state has a strictly positive total parity. Because the intrinsic parity of the emitted pion is negative (-1), the spatial wavefunction of the three-body state must adapt to compensate. To ensure the total parity remains positive, the spatial wavefunction of the dressed state must possess odd parity $((-1)_{\text{intrinsic}} \times (-1)_{\text{spatial}} = +1_{\text{total}})$. In terms of orbital angular momentum, this requires the $pn\pi$ channel to reside in a state with an odd angular momentum quantum number $(\ell = 1, 3, \dots)$. In the Correlated Gaussian framework, this odd spatial parity is enforced by taking the antisymmetric linear combination of the shifted states rather than the symmetric sum:

$$\psi_{pn\pi} = |A, a\rangle - |A, -a\rangle. \tag{61}$$

This gives 9 final overlaps to calculate between the bare state and pion states, for the case of π^0 with spin flip in the first particle, it would be

$$\langle \psi_{pn\pi^0} | \langle \xi_{\pi^0} | \langle \downarrow\uparrow | W | \Psi_{pn} \rangle = \langle \psi_{pn\pi^0} | f({w_{\pi 1}}^{\mathsf{T}} \boldsymbol{r}) \sqrt{2} {w_{\pi 1}}^{\mathsf{T}} r^{+} | \psi_{pn} \rangle. \tag{62}$$

Each overlap depends on the combination of isospin, spin, and spatial structure. The next section shows how to compute these using Gaussian basis functions.

5.7 Evaluation of the Transition Matrix Elements

To calculate the off-diagonal transition elements, such as (62), the integration must be performed over the full three-body coordinate space. However, the initial bare state $|pn\rangle$ depends only on the nucleon-nucleon distance and is independent of the pion coordinates.

To resolve this, the 1×1 correlation matrix of the bare state, $A^{(d)}$, is first promoted to the 2×2 three-body Jacobi space by padding with zeros. The Gaussian form factor of the operator W from equation (45) can then be directly absorbed into the exponents. In the Correlated Gaussian framework, multiplying by a Gaussian is equivalent to adding its correlation matrix.

An effective promoted matrix $\tilde{A}$ is constructed to gather both the close-range nucleon boundaries and the pion emissions:

$$\tilde{A} = \begin{pmatrix} A + 1/b_N^2 & 0 \\ 0 & 0 \end{pmatrix} + \frac{1}{b_\pi^2} w_i w_i{}^{\mathsf{T}}. \tag{63}$$

When computing the coupling matrix element $\langle pn\pi|W|pn\rangle$, the effective matrix $\tilde{A}$ replaces the bare correlation matrix in the overlap formula. Since Gaussian multiplication corresponds to matrix addition in the exponent, the form factor effectively increases the effective width of the Gaussian, confining the overlap to the region where the nucleons are close and the pion is near the emitting nucleon. This encoding allows all spatial integrations to be performed analytically within the Gaussian framework.

6 | Computational Methodology

With the spatial basis, momentum transformations, and coupling operators established, the system is fully prepared to evaluate the Hamiltonian. To isolate the effect of relativistic kinematics, an efficient computational framework is necessary to generate the wavefunction and calculate the ground state energy.

To evaluate the ground state of the deuteron-pion system, a custom C++ simulation was constructed utilizing the Stochastic Variational Method (SVM) [1]. This approach relies on expanding the total wavefunction in a linear combination of Correlated Shifted Gaussians and stochastically optimizing their parameters to minimize the energy expectation value. This choice of basis is advantageous, because it provides analytical matrix elements for the overlaps and spatial interactions, reducing computation time.

6.1 Parameterization and Basis Generation

Each basis state in the trial wavefunction is defined by a multi-dimensional Correlated Gaussian, characterized by a positive-definite correlation matrix A and a spatial shift vector $\boldsymbol{s}$. To ensure that A remains strictly positive-definite during generation, it is constructed as:

$$A = \sum_{i<j=1}^{N} \frac{w_{ij} {w_{ij}}^{\mathsf{T}}}{b_{ij}^2}, \tag{64}$$

where w_{ij} is the coordinate extraction vector that isolates the relative distance between particles i and j, and b_{ij} is a parameter defining the physical range between those particles in units of fm.

To ensure uniform coverage of the parameter space and avoid the clustering, inherent in standard pseudo-random number generators, the parameters b_{ij} are sampled using the quasi-random van der Corput sequence, with different prime bases assigned for each particle pair. The ranges are sampled using an exponential distribution, $b_{ij} = -\ln(u)\, b_N$, where $u \in (0, 1)$ is drawn from the sequence. The characteristic length scale b_N represents the maximum nucleon interaction range and is set to 4 fm.

Because the correlated Gaussian parameter space is nonlinear and prone to local minima, the Nelder-Mead simplex method is particularly advantageous. Unlike gradient-descent algorithms, it does not require the evaluation of analytic derivatives, which would be computationally expensive to recalculate for the full Hamiltonian matrix at every step. Instead, the simplex geometrically adapts to the local energy topology, naturally moving down steep energy valleys and contracting near the true minimum to refine precision.

The shift vector $\boldsymbol{s}^{\mathsf{T}} = \frac{1}{2} {\boldsymbol{r}_0}^{\mathsf{T}} A$, which breaks spherical symmetry to accommodate nonzero orbital angular momentum, is also generated stochastically. The Cartesian components of the shift origin $\boldsymbol{r}_0$ are drawn from a uniform distribution $r_0^i \in (-0.2, 0.2)$. These initial boundaries are utilized solely for random generation, during optimization, both b_{ij} and r_0^i are permitted to move freely outside these bounds to minimize the energy.

6.2 Numerical Stabilization

A common numerical instability in variational methods, occurs when the optimizer pushes particles infinitely far apart to artificially achieve a ground state energy of zero. To prevent this unbounded growth and ensure stable convergence during the initial stages of basis building, a weak harmonic oscillator potential, $V_{\text{trap}} = h_0 r^2$, is added to the diagonal Hamiltonian.

The overlap matrix elements involving this confining potential are computed analytically using equation (16). The trap acts as a temporary physical boundary, forcing the particles to interact. As the basis grows and the nuclear bounds stabilize, the trap strength h_0 is weakened. This ensures that the final, converged physical observables are independent of the artificial confining potential.

6.3 Competitive Search and Optimization

The Gaussian basis is built iteratively. To add the K-th basis state, a large pool, of random candidate states is generated. Each candidate is temporarily appended to the existing basis of size $K-1$, the Hamiltonian and overlap matrices are constructed, and the ground state energy is evaluated. The candidate that yields the lowest overall energy wins the competitive selection and is permanently added to the basis [1].

Once a candidate is selected, it undergoes refinement using the Nelder-Mead algorithm. The algorithm operates on a simplex in either 4- or 6-dimensional parameter space, depending on the system, optimizing the distance parameters b_{ij} and the shift vector components of $\boldsymbol{r}_0$. At each iteration, the vertex with the highest energy is reflected, expanded, or contracted to walk the simplex down the energy gradient, based on a set of rules [3].

6.4 Solving the Generalized Eigenvalue Problem

During both competitive search and Nelder-Mead optimization, the simulation must repeatedly solve the generalized eigenvalue problem:

$$\mathcal{H}c = E\mathcal{N}c, \tag{65}$$

where $\mathcal{H}$ is the block-structured Hamiltonian matrix, $\mathcal{N}$ is the overlap matrix, c is the vector of linear coefficients, and E is the energy. Because the overlap matrix $\mathcal{N}$ is symmetric and strictly positive-definite, the problem is converted into a standard symmetric eigenvalue problem via Cholesky decomposition ($\mathcal{N} = LL^{\mathsf{T}}$):

$$\left(L^{-1}\mathcal{H}L^{-\mathsf{T}}\right)\left(L^{\mathsf{T}}c\right) = E(L^{\mathsf{T}}c). \tag{66}$$

The presence of the overlap matrix $\mathcal{N}$ in the eigenvalue equation is a direct consequence of using a non-orthogonal basis. Because the correlated Gaussians are generated stochastically and independently, they overlap with one another in spatial representation. The matrix $\mathcal{N}$ accounts for this linear dependence to ensure the physical state remains properly normalized.

The Cholesky decomposition effectively orthogonalizes this basis computationally, allowing the standard Jacobi algorithm to find the correct energy eigenstates. The standard symmetric matrix is then diagonalized using the Jacobi eigenvalue algorithm, which iteratively eliminates off-diagonal elements via orthogonal transformations.

The standard Jacobi algorithm operates with $\mathcal{O}(n^3)$ complexity, which represents a significant computational bottleneck when executed hundreds of times per Nelder-Mead step. To accelerate this process, a truncated variant is employed during optimization that restricts the Jacobi sweeps to only the first row of the matrix. This retains sufficient accuracy since we are onely interested in the lowest eigenvalue. After the Nelder-Mead optimization a final, un-truncated diagonalization is performed to obtain the precise ground state energy.

6.5 Execution and Convergence

The basis is constructed in stages. First, the simulation is seeded with 5 geometrically varied Gaussian functions for the bare state. Then, two Gaussian states are competitively selected for each pion channel, and the parameters for each state are optimized to achieve partial convergence. To explore the parameter space while maintaining numerical stability, this competitive search is performed across 7 different harmonic oscillator trap strengths. Subsequently, the entire basis is optimized together. The full Hamiltonian matrix is iteratively evaluated and minimized until the ground state energy converges to within 10^{-4} MeV precision.

7 | Results

Before extracting physical observables, it is necessary to verify the numerical stability of the Stochastic Variational Method. Figure 1 illustrates the convergence of the ground state energy and the charge radius as the size of the Gaussian basis increases.

The stabilization of both observables to within 0.1% of the experimental values confirms that the basis successfully captures the physical structure of the system. To satisfy the 10^{-4} MeV convergence, the algorithm ultimately required $N = 14$ Gaussian states for each of the 9 pion channels and $N = 5$ for the bare state, resulting in a total optimal basis size of 131 Gaussians.

7.1 Model Calibration

With the numerical convergence verified, the parameters S, b_π, and b_N in the form factor (45) must be determined by fitting to experimental data. The model targets the experimental ground state energy of the deuteron, $E_0 = -2.224$ MeV (corresponding to a binding energy of 2.224 MeV), and its charge radius, $r_d = 2.128$ fm [4]. Since there are three fitting parameters but only two target observables, one parameter is fixed: $b_\pi = 1.4$ fm, which corresponds to the Compton wavelength of the pion ($\hbar/m_\pi c \approx 1.43$ fm).

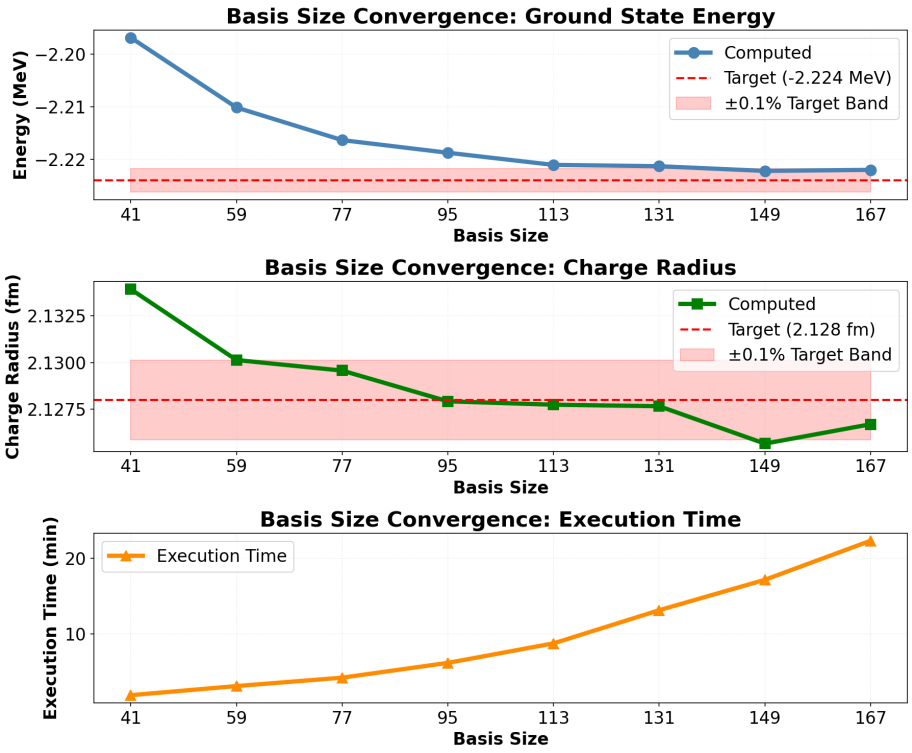

Figure 1: Convergence of the ground state energy and charge radius as a function of the total basis size. Both observables stabilize, demonstrating that the final basis size of 131 Gaussians is sufficient to achieve numerical precision. The total runtime, in seconds, for each of the runs can be seen in the last plot

The remaining parameters, S and b_N, are optimized simultaneously. Figure 2 displays the parameter space, highlighting the specific curves where the calculated energy and radius match experimental values. The intersection of these two target curves defines the unique solution for the system. Based on this calibration, the chosen parameters for the classical calculations are set to $S = 31.29$ MeV and $b_N = 2.24$ fm.

7.2 Relativistic Kinematics

To quantify the effect of relativity on the system, four different configurations of the Hamiltonian were evaluated. Since the kinetic energy is calculated separately for the nucleon pair (K_{pn}) and the pion ($K_{pn\pi}$), the classi-

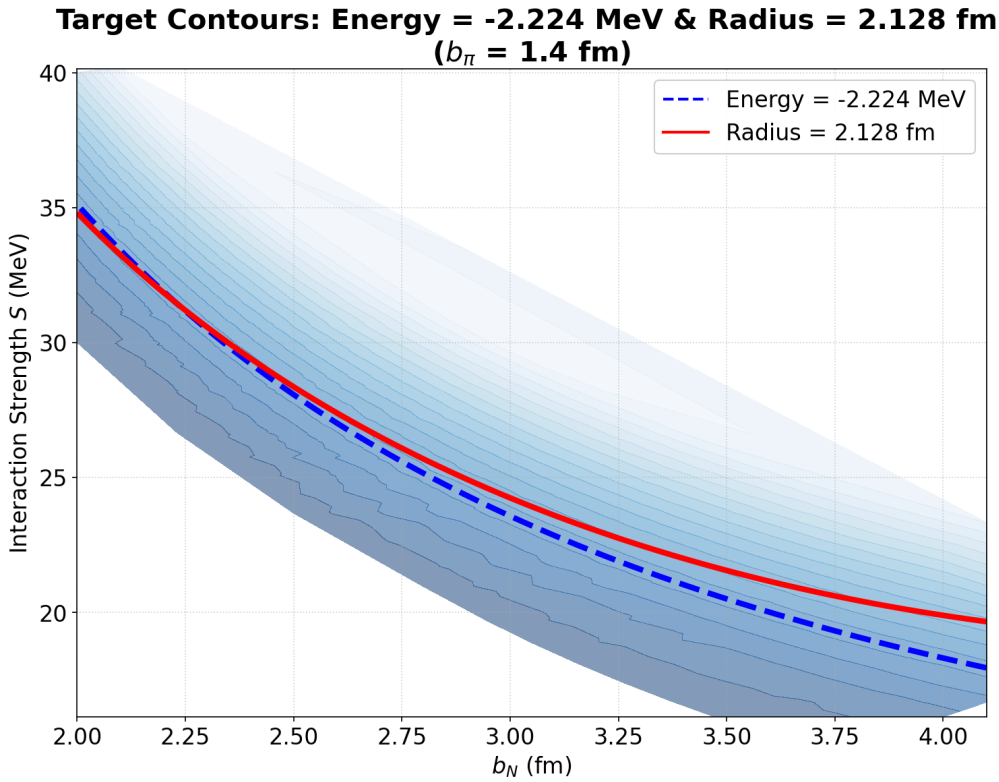

Figure 2: Contour plot of the parameter space for the form factor strength S and the nucleon interaction range b_N. The solid curves indicate the parameter combinations that independently reproduce the experimental deuteron ground state energy ($E_0 = -2.224$ MeV) and charge radius ($r_d = 2.128$ fm). The intersection of these curves yields the optimal parameter set used for subsequent calculations.

cal operator ($p^2/2m$) (31) and the relativistic operator ($\sqrt{p^2+m^2}-m$) (34) can be applied independently to each mass partition. The results of switching these operators using the initially calibrated parameters are shown in Table 1.

Because the pion mass ($m_\pi \approx 140$ MeV) is much smaller than the nucleon mass ($m_N \approx 938$ MeV), pions reach a much higher momentum than the nucleons inside the nucleus. This momentum scale difference makes relativistic effects significant for the pion, while remaining minimal for the heavy nucleons.

Nucleons	**Pion**	E_0 **(MeV)**	r_d **(fm)**	$\langle K \rangle$ **(MeV)**	P_π **(%)**
Classic	Classic	-2.221	2.125	16.78	2.613
Relat.	Classic	-2.633	1.990	18.59	2.930
Classic	Relat.	-6.693	1.550	27.38	5.703
Relat.	Relat.	-7.579	1.483	29.47	6.222

Table 1: Ground state properties using different combinations of classic and relativistic kinetic energy operators. $\langle K \rangle$ is the expectation value of the kinetic energy and P_π is the probability of finding the system in the pion-dressed state.

Beyond the total binding energy, the transition to relativistic kinematics significantly alters the internal structure of the nucleus. As shown in Table 1, applying the relativistic operator to the pion more than doubles the probability of finding the system in the pion-dressed state (P_π), increasing it from approximately 2.6% to 6.2%. Because the relativistic kinetic operator imposes a much smaller energy penalty, than the classical quadratic operator, at high momenta, it becomes energetically favorable for the system, to populate the high-momentum meson-dressed configuration. This demonstrates that relativistic mechanics does not just shift the final energy value, but changes the quantum mechanical composition of the ground state.

Because evaluating the relativistic kinetic energy requires numerical integration over the momentum range from zero to infinity, it is computationally more expensive than evaluating the analytical classical operator. Table 2 details the absolute energy shift to the purely classical baseline, alongside the total computational runtime for each kinematic configuration.

Nucleons	**Pion**	ΔE **(MeV)**	**Runtime (min)**
Classic	Classic	0.000	11.8
Relat.	Classic	-0.411	19.8
Classic	Relat.	-4.471	22.0
Relat.	Relat.	-5.358	30.1

Table 2: Absolute energy shift ($\Delta E = E_0 - E_{\text{classic}}$) and computational runtime for the different combinations of kinetic energy operators. The purely classical configuration serves as the baseline.

To address the overbinding caused by the relativistic pion kinematics, the form factor parameters were re-calibrated specifically for the mixed Hamiltonian (Classical Nucleons, Relativistic Pion). By holding the interaction range fixed at $b_N = 2.24$ fm and targeting the ground state energy ($E_0 = -2.224$ MeV), a new optimal coupling strength was found. Through this recalibration, the optimal parameter that matches the experimental binding energy is found to be $S = 27.19$, resulting in a change of

$$\Delta S = S_{\text{mixed}} - S_{\text{classic}} = 27.19 \text{ MeV} - 31.29 \text{ MeV} = -4.10 \text{ MeV}. \quad (67)$$

This reduction in coupling strength compensates for the diminished kinetic energy of the high-momentum relativistic pion, preventing artificial overbinding.

Comparing the internal properties of the calibrated models clarifies this reduction in coupling strength. While both models now yield the same binding energy, the recalibrated mixed model has a lower expected kinetic energy ($\langle K \rangle = 15.81$ MeV vs. 16.78 MeV). With less kinetic energy pushing the system apart, less potential attraction is needed to bind it, explaining the smaller S.

Additionally, the pion probability, for the recalibrated mixed state, settles at $P_\pi = 3.11\%$, which is noticeably higher than the classical probability of 2.61%. This increase is a consequence of the kinetic energy operators. In the classical framework, the kinetic energy penalty grows quadratically ($p^2/2m$), strongly suppressing fast-moving light particles. Relativistically, this penalty scales linearly at high momentum. With a lower kinetic energy barrier, it becomes easier for the system to access high-momentum states, naturally resulting in a higher pion probability.

To demonstrate the full macroscopic impact of this new parameter set across the entire model space, all four kinematic configurations were re-evaluated utilizing $S = 27.19$ MeV and $b_N = 2.24$ fm. The resulting ground state energies and their respective deviations from the newly calibrated mixed-model baseline are presented in Table 3.

Nucleons	**Pion**	E_0 **(MeV)**	ΔE **(MeV)**
Classic	Classic	-0.219	2.001
Relat.	Classic	-0.326	1.894
Classic	Relat.	-2.220	0.000
Relat.	Relat.	-2.653	-0.433

Table 3: Ground state properties for all kinematic configurations calculated using the re-calibrated parameter set ($S = 27.19$ MeV, $b_N = 2.24$ fm). The Classic-Relativistic configuration now serves as the baseline. As expected, applying these weaker parameters back to the classical Hamiltonian results in underbinding.

8 | Discussion

The results highlight a clear trade-off between computational cost and physical accuracy. Calculating the relativistic kinetic energy for the pion is essential, as it shifts the binding energy by roughly 4.5 MeV. Applying the relativistic operator to the heavy nucleons contributes an additional 0.4 MeV correction. In the context of nuclear binding, a 0.4 MeV shift is physically significant and must be included for precision modeling. However, moving from the mixed model to the full relativistic treatment increases the computational runtime from 22 to 30 minutes. Therefore, while the mixed kinematic model (classical nucleons, relativistic pion) provides an efficient baseline for rapid parameter optimization, the pure relativistic model is required for exact physical results.

The model relies on a few simplifications that should be noted. First, the Coulomb interaction is ignored. While this has minimal effects on the deuteron core, it would become an issue in heavier nuclei where proton repulsion plays a larger role. Furthermore, adding the Coulomb force breaks the isospin symmetry of the system. Because the interaction becomes charge-dependent, the charged ($\pi^{\pm}$) and neutral (π^0) pion channels would no longer be energetically degenerate.

Second, an artificial harmonic trap is used during the basis generation, to prevent the particles from spreading too far apart. Although this trap is gradually weakened, so the final states do not depend on it, it remains a numerical tool rather than a physical one.

Third, the nucleon interaction range b_N is used as a free parameter. In a more realistic model, the nucleons would emit and absorb pions regardless of the distance between each other. The binding energy could then be calculated simply, as the energy difference between the bound two-nucleon state and the isolated, pion-dressed nucleons. However, getting the numerical optimization to reliably find these separated states proved difficult, which is why the Gaussian form factor was used instead.

Future improvements to the model could include two-pion intermediate states. This would allow nucleons to interact through multiple pion exchanges, which is necessary to capture the tensor force. Since adding more pions will increase the computation time, the numerical methods would need to be further optimized to handle the extra load.

Explicit calculations of the deuteron's quadrupole moment could also be introduced. Since the deuteron is not spherical, the tensor component of the pion exchange interaction mixes the S-wave state with a D-wave state. Because the basis utilizes shifted Gaussians, where the stochastic shift vector $\boldsymbol{s}$ inherently breaks spherical symmetry, the trial wavefunction already possesses the capacity to describe this angular momentum mixing. Calculating the quadrupole moment would give another experimental value to fit against, removing the need to fix b_π.

Future work could also investigate heavier mesons to find the exact breakpoint where particles transition from requiring relativistic kinematics to being accurately described by classical mechanics.

9 | Conclusion

This project quantified the relativistic corrections to the ground state of the deuteron, using a nuclear model that includes explicit mesons. By applying the Stochastic Variational Method with Correlated Shifted Gaussians, the system was evaluated using both classical and relativistic kinetic energy operators for the bare and pion-dressed states.

The main finding is that relativistic kinematics are essential for the pion and produce a physically significant correction for the nucleons. Because the pion is very light ($m_\pi \approx 140$ MeV), it reaches relativistic speeds inside the nucleus. Accounting for this, changes the binding energy by approximately 4.5 MeV. In contrast, the much heavier nucleons ($m_N \approx 938$ MeV) experience a smaller relativistic shift of roughly 0.4 MeV.

These results point to a limitation in standard low-energy nuclear models, which typically apply classical kinetic energy operators to all particles. While this classical approach works well for heavy nucleons, it fails to capture the correct dynamics of light mesons. If a computational model includes explicit mesons, it must use relativistic operators for those light particles to get accurate physical results.

Ultimately, while a fully relativistic model provides the most accurate physical description, a mixed kinematic approach, using classical operators for the heavy nucleons and relativistic operators for the pions, captures the majority of the relativistic energy shift, while reducing computation time. This established framework provides a solid and efficient starting point for future research into multi-pion systems and heavier nuclei.

Bibliography

[1] Suzuki, Y., & Varga, K. (1998). *Stochastic variational approach to quantum-mechanical few-body problems*. Springer.

[2] Fedorov, D. V. (2017). Analytic matrix elements and gradients with shifted correlated Gaussians. *Few-Body Systems*, *58*(1), 21.

[3] Nelder, J. A., & Mead, R. (1965). A simplex method for function minimization. *The Computer Journal*, *7*(4), 308–313.

[4] Ericson, T. E. O. (1984). The deuteron properties. *Nuclear Physics A*, *416*, 281–298.

[5] Fedorov, D. V. (2020). A nuclear model with explicit mesons. *Few-Body Systems*, *61*(4), 43.

[6] Griffiths, D. J., & Schroeter, D. F. (2018). *Introduction to quantum mechanics* (3rd ed.). Cambridge University Press.

[7] Navas, S., et al. (Particle Data Group). (2024). Review of particle physics. *Physical Review D*, *110*(3), 030001. https://pdg.lbl.gov/2024/listings/particle_properties.html

A | Derivation of the Coupling Operator

Applying the full coupling operator to the bare state wavefunction, and eliminating terms that would have no overlap, reveals all 9 possible pion states used in the project. The spin and isospin parts determine the states and their relative coefficients, so we apply the operator to these parts first and leave the spatial form factor evaluation for last.

$$\begin{aligned} W|\chi\rangle|\xi\rangle &= [W_1 + W_2]\,|\uparrow\uparrow\rangle\frac{1}{\sqrt{2}}\left(|pn\rangle - |np\rangle\right) \\ &= [(\boldsymbol{\tau}_1\cdot\boldsymbol{\pi})(\boldsymbol{\sigma}_1\cdot {w_{\pi 1}}^{\mathsf{T}}\boldsymbol{r})f({w_{\pi 1}}^{\mathsf{T}}\boldsymbol{r}) + (\boldsymbol{\tau}_2\cdot\boldsymbol{\pi})(\boldsymbol{\sigma}_2\cdot {w_{\pi 2}}^{\mathsf{T}}\boldsymbol{r})f({w_{\pi 2}}^{\mathsf{T}}\boldsymbol{r})] \\ &\quad \frac{1}{\sqrt{2}}\left(|pn\rangle - |np\rangle\right)|\uparrow\uparrow\rangle \end{aligned} \tag{68}$$

First, we evaluate the isospin operator $(\boldsymbol{\tau}\cdot\boldsymbol{\pi}) = \tau^0\pi^0 + \sqrt{2}\tau^-\pi^+ + \sqrt{2}\tau^+\pi^-$ on the antisymmetric isospin singlet $|\xi\rangle$. For the first nucleon, this yields:

$$\begin{aligned} (\boldsymbol{\tau}_1\cdot\boldsymbol{\pi})\frac{1}{\sqrt{2}}\left(|pn\rangle - |np\rangle\right) &= \pi^0\frac{1}{\sqrt{2}}\left(|pn\rangle + |np\rangle\right) + \pi^+\left(-|nn\rangle\right) + \pi^-\left(|pp\rangle\right) \\ &\equiv \pi^0|\xi_{sym}\rangle - \pi^+|nn\rangle + \pi^-|pp\rangle. \end{aligned} \tag{69}$$

For the second nucleon, applying the operator yields a relative minus sign across all channels due to the antisymmetry of the initial state:

$$\begin{aligned} (\boldsymbol{\tau}_2\cdot\boldsymbol{\pi})\frac{1}{\sqrt{2}}\left(|pn\rangle - |np\rangle\right) &= \pi^0\frac{1}{\sqrt{2}}\left(-|pn\rangle - |np\rangle\right) + \pi^+\left(|nn\rangle\right) + \pi^-\left(-|pp\rangle\right) \\ &= -\pi^0|\xi_{sym}\rangle + \pi^+|nn\rangle - \pi^-|pp\rangle. \end{aligned} \tag{70}$$

Next, we evaluate the spin operator $(\boldsymbol{\sigma}\cdot {w}^{\mathsf{T}}\boldsymbol{r}) = \sigma^0 {w}^{\mathsf{T}} r^0 + \sqrt{2}\sigma^- {w}^{\mathsf{T}} r^+ + \sqrt{2}\sigma^+ {w}^{\mathsf{T}} r^-$ on the initial spin triplet $|\uparrow\uparrow\rangle$. Because both nucleons are already in the spin-up state, the σ^+ raising operator annihilates the state

entirely. For the first and second nucleon respectively, the non-zero terms are:

$$(\boldsymbol{\sigma}_1 \cdot {w_{\pi 1}}^{\mathsf{T}} \boldsymbol{r})|\uparrow\uparrow\rangle = {w_{\pi 1}}^{\mathsf{T}} r^0 |\uparrow\uparrow\rangle + \sqrt{2} {w_{\pi 1}}^{\mathsf{T}} r^+ |\downarrow\uparrow\rangle, \tag{71}$$

$$(\boldsymbol{\sigma}_2 \cdot {w_{\pi 2}}^{\mathsf{T}} \boldsymbol{r})|\uparrow\uparrow\rangle = {w_{\pi 2}}^{\mathsf{T}} r^0 |\uparrow\uparrow\rangle + \sqrt{2} {w_{\pi 2}}^{\mathsf{T}} r^+ |\uparrow\downarrow\rangle. \tag{72}$$

Now we assemble the isospin, spin, and spatial form factors back into the total expression. Let $f_1 = f({w_{\pi 1}}^{\mathsf{T}} \boldsymbol{r})$ and $f_2 = f({w_{\pi 2}}^{\mathsf{T}} \boldsymbol{r})$ for brevity. By grouping the terms by the emitted pion type, we obtain the final 9 intermediate dressed states:

$$\begin{aligned} W|\chi\rangle|\xi\rangle = \pi^0|\xi_{sym}\rangle \otimes \left[\left(f_1 {w_{\pi 1}}^{\mathsf{T}} r^0 - f_2 {w_{\pi 2}}^{\mathsf{T}} r^0 \right) |\uparrow\uparrow\rangle + \sqrt{2} f_1 {w_{\pi 1}}^{\mathsf{T}} r^+ |\downarrow\uparrow\rangle - \sqrt{2} f_2 {w_{\pi 2}}^{\mathsf{T}} r^+ |\uparrow\downarrow\rangle \right] \\ + \pi^+|nn\rangle \otimes \left[\left(-f_1 {w_{\pi 1}}^{\mathsf{T}} r^0 + f_2 {w_{\pi 2}}^{\mathsf{T}} r^0 \right) |\uparrow\uparrow\rangle - \sqrt{2} f_1 {w_{\pi 1}}^{\mathsf{T}} r^+ |\downarrow\uparrow\rangle + \sqrt{2} f_2 {w_{\pi 2}}^{\mathsf{T}} r^+ |\uparrow\downarrow\rangle \right] \\ + \pi^-|pp\rangle \otimes \left[\left(f_1 {w_{\pi 1}}^{\mathsf{T}} r^0 - f_2 {w_{\pi 2}}^{\mathsf{T}} r^0 \right) |\uparrow\uparrow\rangle + \sqrt{2} f_1 {w_{\pi 1}}^{\mathsf{T}} r^+ |\downarrow\uparrow\rangle - \sqrt{2} f_2 {w_{\pi 2}}^{\mathsf{T}} r^+ |\uparrow\downarrow\rangle \right]. \end{aligned} \tag{73}$$

This explicit expansion clearly demonstrates how the 3 pion channels (π^0, π^+, π^-) couple to the 3 spin configurations $(|\uparrow\uparrow\rangle, |\downarrow\uparrow\rangle, |\uparrow\downarrow\rangle)$, generating the $3 \times 3 = 9$ unique spatial matrix elements required to construct the transition blocks of the Hamiltonian.

B | Source Code

The complete C++ source code for the Stochastic Variational Method simulation, alongside scripts for data analysis and visualization, is publicly available in a GitHub repository:

https://github.com/Moth-0/Relativistic-Kinematics-of-Pion-Dressed-Deuteron.